

# DIELECTRIC, PIEZOELECTRIC, AND ELASTIC PROPERTIES OF $\text{BaTiO}_3/\text{SrTiO}_3$ FERROELECTRIC SUPERLATTICES FROM FIRST PRINCIPLES

ALEXANDER I. LEBEDEV\*

*Physics Department, Moscow State University  
119991 Moscow, Russia  
swan@scon155.phys.msu.ru*

Received 7 November 2011

Published 27 February 2012

The effect of epitaxial strain on the phonon spectra, crystal structure, spontaneous polarization, dielectric, piezoelectric, and elastic properties of (001)-oriented ferroelectric  $(\text{BaTiO}_3)_m/(\text{SrTiO}_3)_n$  superlattices ( $m = n = 1-4$ ) was studied using the first-principles density functional theory. The ground state of free-standing superlattices is the monoclinic  $Cm$  polar phase. Under the in-plane biaxial compressive strain, it transforms to tetragonal  $P4mm$  polar phase, and under the in-plane biaxial tensile strain, it transforms to orthorhombic  $Amm2$  polar phase. When changing the in-plane lattice parameter, a softening of several optical and acoustic modes appears at the boundaries between the polar phases, and corresponding components of dielectric, piezoelectric, and elastic tensors diverge critically. The comparison of the mixing enthalpy of disordered  $\text{Ba}_{0.5}\text{Sr}_{0.5}\text{TiO}_3$  solid solution modeled using two special quasirandom structures SQS-4 with the mixing enthalpy of the superlattices reveals a tendency of the  $\text{BaTiO}_3\text{-SrTiO}_3$  system to short-range ordering and shows that these superlattices are thermodynamically quite stable.

*Keywords:* Ferroelectric superlattices; first-principles calculations.

PACS number(s): 64.60.-i, 68.65.Cd, 77.84.Dy, 81.05.Zx

## 1. Introduction

The success in creating of ferroelectric superlattices with a layer thickness controlled with an accuracy of one monolayer offers new opportunities for design of new ferroelectric multifunctional materials with high spontaneous polarization, Curie temperature, dielectric constant, and large dielectric and optical nonlinearities. Because of many problems encountered in the growth and experimental studies of ferroelectric superlattices, first-principles calculations of their physical properties can be used to reveal new promising fields of investigations and applications of these materials.

Earlier studies of thin epitaxial films of ferroelectrics with the perovskite structure have shown that their properties differ strongly from those of bulk crystals. It was established that substrate-induced strain (epitaxial strain) has a strong influence on the properties of films. Due to strong coupling between strain and polarization, this strain changes significantly the phase transition temperature and can induce unusual polar states in thin films.<sup>1-4</sup>

To date, the most experimentally studied ferroelectric superlattice is the  $\text{BaTiO}_3/\text{SrTiO}_3$  (BTO/STO) one.<sup>5-32</sup> Studies of these superlattices from first principles<sup>24,25,33-44</sup> have established main

\*Corresponding author.

factors responsible for the formation of their polar structure. The specific feature of the superlattice is that the strains induced in it by the lattice mismatch between  $\text{BaTiO}_3$  and  $\text{SrTiO}_3$  and by the substrate result in concurrency of equilibrium polar structures in neighboring layers, so that the polar structure of the superlattice can be tetragonal, monoclinic, or orthorhombic, depending on the mechanical boundary conditions at the interface with the substrate.

Although some properties of BTO/STO superlattices have been already studied, a number of problems remain unresolved. For instance, first-principles study of dielectric properties of these superlattices<sup>36,37</sup> have found only  $P4mm$  and  $Cm$  polar phases, whereas the  $Amm2$  phase, which is characteristic for stretched films of  $\text{BaTiO}_3$ ,<sup>2</sup>  $\text{SrTiO}_3$ ,<sup>45</sup> and for  $\text{PbTiO}_3/\text{PbZrO}_3$  superlattices,<sup>46</sup> was not observed. The piezoelectric properties were calculated only for  $\text{PbTiO}_3/\text{PbZrO}_3$  superlattice;<sup>47</sup> for BTO/STO superlattices these data are absent. Finally, the elastic properties of ferroelectric superlattices and their behavior at the boundaries between different polar phases have not been studied at all.

In this work, first-principles density functional calculations of the phonon spectra, crystal structure, spontaneous polarization, dielectric, piezoelectric, and elastic properties for polar phases of (001)-oriented  $(\text{BTO})_m/(\text{STO})_n$  superlattices (SL  $m/n$ ) with  $m = n = 1-4$  are performed. The influence of compressive and tensile epitaxial strain on the structure and properties of polar phases is studied in details for  $(\text{BTO})_1/(\text{STO})_1$  superlattice. The stability ranges of tetragonal, monoclinic, and orthorhombic phases are determined. The critical behavior of static dielectric, piezoelectric, and elastic tensors at the boundaries between different polar phases are studied. The ferroelastic type of the phase transitions between the polar phases is established. In addition, an

important question about the thermodynamic stability of BTO/STO superlattices is considered.

The remainder of this paper is organized as follows. In Sec. 2, we give the details of our calculations. Next, we present the results for the ground state (Sec. 3.1) and the polarization (Sec. 3.2) of  $(\text{BTO})_n/(\text{STO})_n$  superlattices. Dielectric, piezoelectric, and elastic properties of  $(\text{BTO})_1/(\text{STO})_1$  superlattice are described in Secs. 3.3–3.5, respectively. The thermodynamic stability of the superlattices is analyzed in Sec. 3.6. The obtained results are discussed in Sec. 4.

## 2. Calculation Details

The calculations were performed within the first-principles density functional theory (DFT) with pseudopotentials and a plane-wave basis set as implemented in ABINIT software.<sup>49</sup> The local density approximation (LDA) for the exchange-correlation functional<sup>50</sup> was used. Optimized separable nonlocal pseudopotentials<sup>51</sup> were constructed using the OPIUM software,<sup>52</sup> to improve the transferability of pseudopotentials, the local potential correction was added according to Ref. 53. Parameters used for construction of pseudopotentials are given in Table 1; the results of testing of these pseudopotentials and other details of calculations can be found in Ref. 48. The plane-wave cut-off energy was 30 Ha (816 eV). The integration over the Brillouin zone was performed with a  $8 \times 8 \times 4$  Monkhorst–Pack mesh. The relaxations of the atomic positions and the unit cell parameters were stopped when the Hellmann–Feynman forces were below  $5 \cdot 10^{-6}$  Ha/Bohr (0.25 meV/Å).

The lattice parameters calculated using the pseudopotentials were  $a = 7.3506$  Bohr (3.8898 Å) for bulk  $\text{SrTiO}_3$  and  $a = 7.4923$  Bohr (3.9648 Å),  $c = 7.5732$  Bohr (4.0075 Å) for tetragonal  $\text{BaTiO}_3$ .

Table 1. Parameters used for construction of pseudopotentials.<sup>48</sup> Nonrelativistic generation scheme was used for Sr, Ti, and O atoms, and scalar-relativistic generation scheme was used for the Ba atom. All parameters are in Hartree atomic units except for the energy  $V_{\text{loc}}$ , which is in Ry.

Atom	Configuration	$r_s$	$r_p$	$r_d$	$q_s$	$q_p$	$q_d$	$r_{\text{min}}$	$r_{\text{max}}$	$V_{\text{loc}}$
Sr	$4s^2 4p^6 4d^0 5s^0$	1.68	1.74	1.68	7.07	7.07	7.07	0.01	1.52	1.5
Ba	$5s^2 5p^6 5d^0 6s^0$	1.85	1.78	1.83	7.07	7.07	7.07	0.01	1.68	1.95
Ti	$3s^2 3p^6 3d^0 4s^0$	1.48	1.72	1.84	7.07	7.07	7.07	0.01	1.41	2.65
O	$2s^2 2p^4 3d^0$	1.40	1.55	1.40	7.07	7.57	7.07	—	—	—

Slight underestimation of the lattice parameters (in our case by 0.4–0.7% compared to the experimental data) is a known problem of LDA calculations.

The calculations were performed on two structures: supercells of  $1 \times 1 \times 2n$  perovskite unit cells for (001)-oriented  $(\text{BTO})_n/(\text{STO})_n$  superlattices ( $n = 1-4$ ) and two special quasirandom structures (SQS) for  $\text{Ba}_{0.5}\text{Sr}_{0.5}\text{TiO}_3$  solid solution; the construction of SQSs is described in Sec. 3.6.

Phonon spectra, dielectric, piezoelectric, and elastic properties of the superlattices were calculated within the DFT perturbation theory. Phonon contribution to the dielectric constant was calculated from phonon frequencies and oscillator strengths.<sup>54</sup> The Berry phase method<sup>55</sup> was used to calculate the spontaneous polarization  $P_s$ .

As the layers of the superlattices are epitaxially grown on (001)-oriented substrate with a cubic structure, the calculations were performed for pseudotetragonal unit cells in which two in-plane translation vectors have the same length  $a_0$  and all three translation vectors are perpendicular to each other. This means that for monoclinic and orthorhombic phases (with  $Cm$  and  $Amm2$  space groups) small deviations of the angles between the translation vectors from  $90^\circ$  (which were typically less than  $0.07^\circ$ ) were neglected. As was checked, this does not influence much the results.

### 3. Results

#### 3.1. Ground state of epitaxially strained superlattices

The lattice mismatch between  $\text{BaTiO}_3$  and  $\text{SrTiO}_3$  creates tensile biaxial strain in  $\text{SrTiO}_3$  layers and compressive biaxial strain in  $\text{BaTiO}_3$  layers of free-standing BTO/STO superlattice. If the layers were isolated, these strains would result in appearance of the in-plane spontaneous polarization in  $\text{SrTiO}_3$  ( $Amm2$  space group) and in increase of the out-of-plane polarization in  $\text{BaTiO}_3$  layers ( $Cm$  or  $P4mm$  space groups).<sup>1-3</sup> As the polar state with strong local variations of polarization is energetically unfavorable,<sup>33</sup> the structure of the polar ground state of the superlattice requires special consideration. Earlier studies of BTO/STO<sup>36,37</sup> and  $\text{PbTiO}_3/\text{PbZrO}_3$ <sup>46</sup> superlattices have demonstrated that both the magnitude and orientation of polarization depend also on the substrate-induced (epitaxial) strain in superlattices.

The ground state of BTO/STO superlattice was searched as follows. For a set of in-plane lattice parameters  $a_0$ , which were varied from 7.35 to 7.50 Bohr, we first calculated the equilibrium structure of the paraelectric phase with  $P4/mmm$  space group by minimizing the Hellmann–Feynman forces. The phonon frequencies at the  $\Gamma$  point were then calculated for these structures. It is known that the ground state of any crystal is characterized by positive values of all optical phonon frequencies at all points of the Brillouin zone. So, if the structure under consideration exhibited unstable phonons (with imaginary phonon frequencies), the atomic positions in it were slightly distorted according to the eigenvector of the most unstable mode, and a new search for the equilibrium structure was initiated. The phonon frequencies calculation and the search for equilibrium structure were repeated until the structure with all positive phonon frequencies was found.

It should be noted that the only unstable mode in the paraelectric  $P4/mmm$  phase of  $(\text{BTO})_1/(\text{STO})_1$  superlattice is the ferroelectric one at the  $\Gamma$  point. The well-known structural instability of  $\text{SrTiO}_3$  associated with the  $R_{25}$  phonon mode at the boundary of the Brillouin zone disappears in the superlattice: the frequency of the corresponding phonon at the  $M$  point of the folded Brillouin zone (to which the  $R$  point transforms when doubling the  $c$  lattice parameter) is  $55 \text{ cm}^{-1}$  for 1/1 free-standing superlattice and  $61 \text{ cm}^{-1}$  for 1/1 superlattice grown on  $\text{SrTiO}_3$  substrate (see Fig. 1).

The phonon spectra calculations show that in 1/1 superlattice grown on  $\text{SrTiO}_3$  substrate (compressive epitaxial strain, the in-plane lattice parameter  $a_0$  is equal to that of cubic strontium titanate) the tetragonal polar phase with  $P4mm$  space group is the ground state (Fig. 1). For free-standing superlattice, the  $P4mm$  structure is unstable and transforms to monoclinic  $Cm$  polar one. Under tensile epitaxial strain ( $a_0 = 7.46$  Bohr), the orthorhombic  $Amm2$  polar phase is the most stable one for 1/1 superlattice. This means that the variation of  $a_0$  (for example, by growing the superlattice on different substrates) can be used to control the polar state of the superlattice.

In order to determine accurately the location of the boundaries between  $P4mm$  and  $Cm$  phases and between  $Cm$  and  $Amm2$  phases for 1/1 superlattice, the ground state was calculated for a set of in-plane lattice parameters  $a_0$ , and for each of these

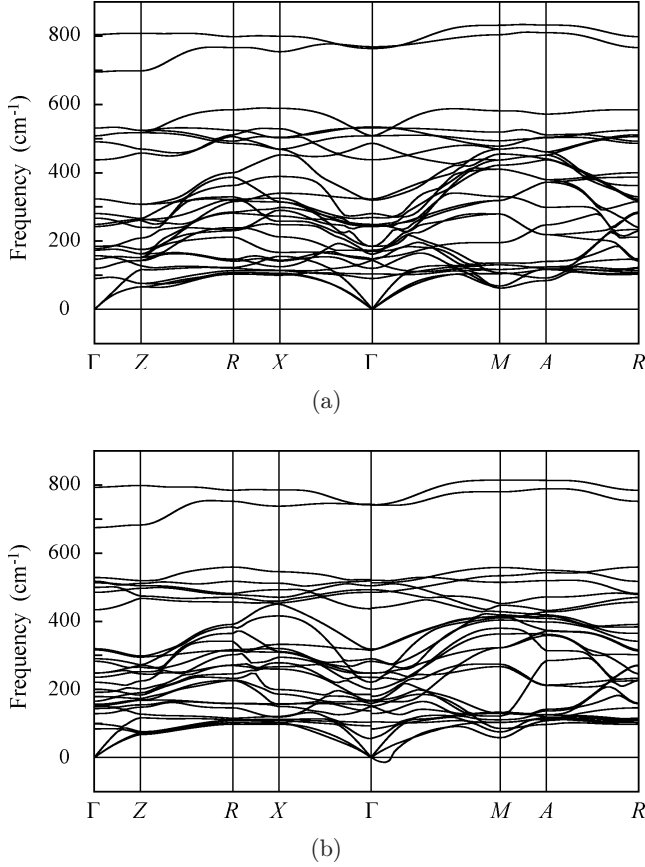


Fig. 1. Phonon spectra for (a) the  $P4mm$  phase of  $(\text{BTO})_1/(\text{STO})_1$  superlattice grown on  $\text{SrTiO}_3$  substrate ( $a_0 = 7.3506$  Bohr) and (b) the  $Cm$  phase of the same, free-standing superlattice ( $a_0 = 7.4461$  Bohr).

structures the phonon frequencies at the  $\Gamma$  point were computed. The dependence of four lowest phonon frequencies on the  $a_0$  parameter is plotted in Fig. 2. It is seen that the frequency of a doubly degenerate  $E$  mode decreases critically when approaching the boundary between  $P4mm$  and  $Cm$  phases from the tetragonal phase. After transition to the monoclinic phase two nondegenerate  $A'$  and  $A''$  soft modes appear in the phonon spectrum; the first of these modes becomes soft again when approaching the boundary between  $Cm$  and  $Amm2$  phases. The soft phonon mode in the  $Amm2$  phase has the  $B_1$  symmetry.

Extrapolation of the squared frequencies of soft ferroelectric modes ( $E$  mode in the  $P4mm$  phase,  $A'$  mode in the  $Cm$  phase, and  $B_1$  mode in the  $Amm2$  phase) as a function of  $a_0$  to zero gives the in-plane lattice parameters corresponding to the boundaries between different polar phases. The  $P4mm$ – $Cm$  boundary is at  $a_0 = 7.4023$  Bohr when extrapolating

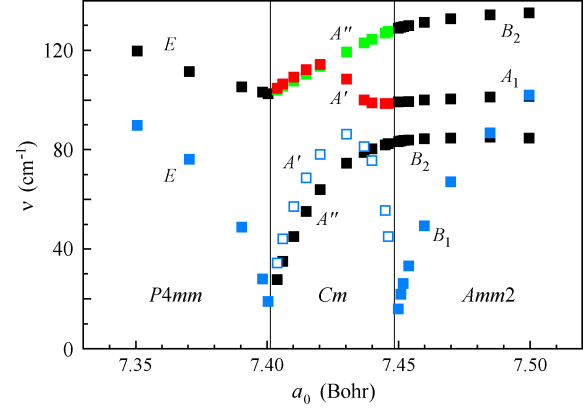


Fig. 2. (Color online) Frequencies of four lowest phonon modes at the  $\Gamma$  point for polar phases of  $(\text{BTO})_1/(\text{STO})_1$  superlattice as a function of the in-plane lattice parameter  $a_0$ . The labels near the points indicate the symmetry of modes. Vertical lines indicate the phase boundaries.

from the tetragonal phase and at  $7.4001$  Bohr when extrapolating from the monoclinic phase. The  $Cm$ – $Amm2$  boundary is at  $a_0 = 7.4489$  Bohr when extrapolating from the orthorhombic phase and at  $7.4483$  Bohr when extrapolating from the monoclinic phase. Small difference between the values obtained from extrapolation from two sides of the boundary means that both phase transitions are close to the second-order ones. Taking into account that a zero in-plane strain in polar superlattice corresponds to the in-plane lattice parameter of  $a_0 = 7.4462$  Bohr, we get the values of  $-0.605\%$  and  $+0.032\%$  for the misfit strains corresponding to the phase boundaries.

Comparison of the energies of different polar phases and calculation of the phonon frequencies at the  $\Gamma$  point for  $(\text{BTO})_2/(\text{STO})_2$  and  $(\text{BTO})_3/(\text{STO})_3$  superlattices shows that the same  $P4mm$ ,  $Cm$ , and  $Amm2$  phases has the lowest energy, respectively, in superlattices grown on  $\text{SrTiO}_3$ , free-standing superlattices, and superlattices grown on the substrate with  $a_0 = 7.46$  Bohr.

### 3.2. Spontaneous polarization

The calculated spontaneous polarization for free-standing and substrate-supported superlattices, tetragonal  $\text{BaTiO}_3$ , and disordered  $\text{Ba}_{0.5}\text{Sr}_{0.5}\text{TiO}_3$  solid solution modeled using SQS-4 structures (see Sec. 3.6) are given in Table 2.

As was established in Sec. 3.1, the tetragonal  $P4mm$  phase with the polarization vector normal

Table 2. Spontaneous polarization (in  $\text{C}/\text{m}^2$ ) for BTO/STO superlattices with different thickness of layers, two SQS-4 structures used for modeling of disordered  $\text{Ba}_{0.5}\text{Sr}_{0.5}\text{TiO}_3$  solid solution, and tetragonal barium titanate. The in-plane lattice parameters  $a_0$  (in Bohr) for superlattices are also presented.

Structure	SL1/1		SL2/2		SL3/3		SL4/4		SQS-4a	SQS-4b	BaTiO <sub>3</sub>
	$[xxz]$	$[001]^a$	$[xxz]$	$[001]^a$	$[xxz]$	$[001]^a$	$[xxz]$	$[001]^a$	$[111]$	$[001]$	$[001]$
$P_z$	0.061	0.277	0.113	0.293	0.146	0.302	0.157	0.307	0.130	0.206	0.259
$P_x = P_y$	0.165	0	0.159	0	0.150	0	0.144	0	0.130	0	0
$a_0$	7.4461	7.3506	7.4432	7.3506	7.4403	7.3506	7.4391	7.3506			

<sup>a</sup>Superlattices grown on  $\text{SrTiO}_3$  substrate.

to the layers is the ground state for BTO/STO superlattices grown on  $\text{SrTiO}_3$  substrate. The calculations shows that in these superlattices the spontaneous polarization  $P_s$  increases monotonically from  $0.277 \text{ C}/\text{m}^2$  to  $0.307 \text{ C}/\text{m}^2$  as the layer thickness is increased from  $n = 1$  to 4 unit cells (see Table 2). The obtained  $P_s$  values agree well with the value of  $0.28 \text{ C}/\text{m}^2$  estimated from the data of Ref. 33 for the superlattice with equal thickness of  $\text{BaTiO}_3$  and  $\text{SrTiO}_3$  layers; the  $P_s$  value of  $0.259 \text{ C}/\text{m}^2$  for tetragonal  $\text{BaTiO}_3$  agrees well with the value of  $0.250 \text{ C}/\text{m}^2$  reported in Ref. 33. As follows from Table 2, for all superlattices the  $P_s$  values are larger than those for  $\text{Ba}_{0.5}\text{Sr}_{0.5}\text{TiO}_3$  solid solution; for superlattices grown on  $\text{SrTiO}_3$  substrates they are even larger than  $P_s$  of tetragonal  $\text{BaTiO}_3$ . These results agree with experiment<sup>13</sup> and results of previous calculations.<sup>33,42</sup>

For free-standing superlattices, the monoclinic  $Cm$  phase is the ground state; the components of the polarization vector in this phase are also given in Table 2. It is seen that the polarization is rotated continuously in the  $(\bar{1}10)$  plane and the magnitude of polarization increases with increasing  $n$ .

For biaxially stretched superlattices, the  $Amm2$  phase is the ground state and the polarization vector is oriented along  $[110]$  direction of the reference tetragonal  $P4/mmm$  structure of the paraelectric phase.

The in-plane and out-of-plane components of the polarization for 1/1 superlattice are plotted as a function of the in-plane lattice parameter  $a_0$  in Fig. 3. Extrapolation of the  $P_\perp^2$  and  $P_z^2$  dependence on  $a_0$  to zero gives the positions of the  $P4mm-Cm$  and  $Cm-Amm2$  phase boundaries. Their values,  $a_0 = 7.4018 \text{ Bohr}$  and  $a_0 = 7.4492 \text{ Bohr}$ , are very close to those obtained in Sec. 3.1 from the frequencies of soft modes.

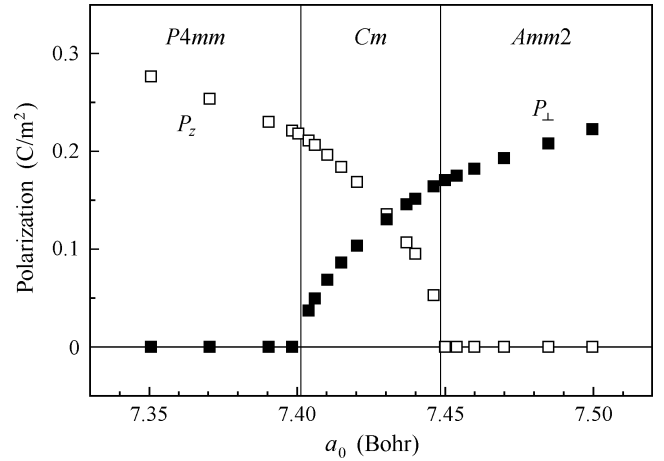


Fig. 3. The in-plane ( $P_\perp$ ) and out-of-plane ( $P_z$ ) components of polarization for  $(\text{BTO})_1/(\text{STO})_1$  superlattice as a function of the in-plane lattice parameter  $a_0$ . Vertical lines indicate the phase boundaries.

### 3.3. Dielectric properties

The eigenvalues of the static dielectric constant tensor  $\varepsilon_{ij}$  ( $i, j = 1, 2, 3$ ) for  $(\text{BTO})_1/(\text{STO})_1$  superlattice as a function of the in-plane lattice parameter  $a_0$  are shown in Fig. 4. In the tetragonal phase, the eigenvectors of the  $\varepsilon_{ij}$  tensor coincide with crystallographic axes and  $\varepsilon_{11} = \varepsilon_{22}$ . So, the dielectric properties of this phase are described by two non-zero independent parameters,  $\varepsilon_{11}$  and  $\varepsilon_{33}$ .

In the monoclinic phase, the polarization vector rotates monotonically in the  $(110)$  plane; all three eigenvectors of the  $\varepsilon_{ij}$  tensor are different and do not coincide with crystallographic axes of the reference tetragonal structure. As all nine components of the  $\varepsilon_{ij}$  tensor in this coordinate system are nonzero for the  $Cm$  phase, the most compact way to describe the properties of this tensor is to present its eigenvalues. In the  $Cm$  phase, the direction of the eigenvector corresponding to the smallest eigenvalue is

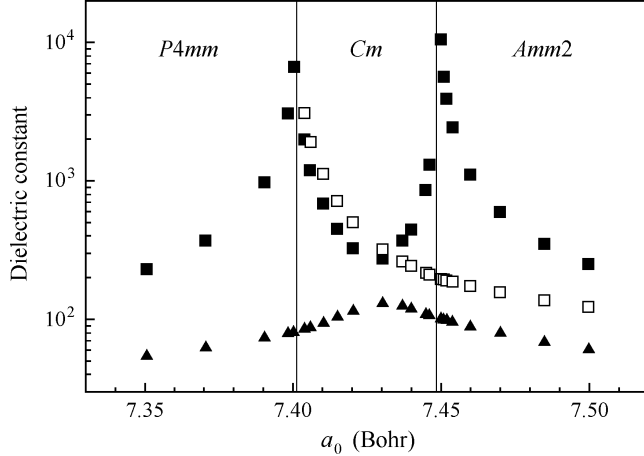


Fig. 4. Eigenvalues of the static dielectric constant tensor  $\varepsilon_{ij}$  for  $(\text{BTO})_1/(\text{STO})_1$  superlattice as a function of the in-plane lattice parameter  $a_0$ . Vertical lines indicate the phase boundaries.

close, but do not coincide with the direction of the polarization.

In the orthorhombic phase, the eigenvectors of the  $\varepsilon_{ij}$  tensor are oriented along the  $[110]$ ,  $[\bar{1}10]$  and,  $[001]$  directions of the reference tetragonal structure. The direction of the eigenvector corresponding to the smallest eigenvalue coincides with the polarization vector and the direction of eigenvector corresponding to the largest eigenvalue is  $[001]$ .

As follows from Fig. 4, at least one of the eigenvalues of the  $\varepsilon_{ij}$  tensor diverges critically at the  $P4mm-Cm$  and  $Cm-Amm2$  boundaries as the in-plane lattice parameter  $a_0$  is changed. When approaching the  $P4mm-Cm$  boundary from the tetragonal phase, the  $\varepsilon_{11} = \varepsilon_{22}$  components of this tensor diverge as the polarization vector  $\mathbf{P}_s \parallel [001]$  becomes less stable against its rotation in the  $(110)$  plane. When approaching the  $Cm-Amm2$  boundary from the orthorhombic phase, the  $\varepsilon_{33}$  value diverges as the polarization vector  $\mathbf{P}_s \parallel [110]$  becomes less stable against its rotation in the same plane.

### 3.4. Piezoelectric properties

Due to high sensitivity of both magnitude and orientation of the polarization vector in superlattices to epitaxial strain, we can expect them to be good piezoelectrics. It is known that anomalously high piezoelectric moduli found in some ferroelectrics like  $\text{PbZr}_{1-x}\text{Ti}_x\text{O}_3$  near the morphotropic phase boundary are due to the ease of strain-induced rotation of polarization in the intermediate

monoclinic phase.<sup>56,57</sup> A similar situation appears in the monoclinic phase of BTO/STO superlattice. To our knowledge, the piezoelectric properties of BTO/STO superlattices have not been studied so far neither experimentally, nor theoretically. The only superlattice, for which some piezoelectric properties were calculated, is the  $\text{PbTiO}_3/\text{PbZrO}_3$  1/1 superlattice,<sup>58</sup> which was used to simulate the properties of  $\text{PbTi}_{0.5}\text{Zr}_{0.5}\text{O}_3$  solid solution.

The largest piezoelectric stress moduli  $e_{i\nu}$  ( $i = 1, 2, 3; \nu = 1-6$ ) calculated for the  $P4mm$  phase of  $(\text{BTO})_1/(\text{STO})_1$  superlattice grown on  $\text{SrTiO}_3$  substrate and for the  $Cm$  phase of the same free-standing superlattice are given in Table 3. It is seen that in tetragonal phases of the superlattice and  $\text{BaTiO}_3$  the  $e_{33}$  moduli do not differ much. However in the monoclinic phase, which is the ground state for free-standing superlattice, the  $e_{33}$  value is five times larger. Even stronger effect can be seen for the  $d_{33}$  piezoelectric strain coefficient ( $d_{i\nu} = \sum_{\mu=1}^6 e_{i\mu} S_{\mu\nu}$ ), which is a result of an 1.5-fold increase in the elastic compliance modulus  $S_{33}$  in the monoclinic phase (see Sec. 3.5).

The piezoelectric moduli  $e_{i\nu}$  in polar phases of  $(\text{BTO})_1/(\text{STO})_1$  superlattice as a function of the in-plane lattice parameter are shown in Fig. 5. According to the symmetry, in the tetragonal phase the piezoelectric tensor has three independent and five nonzero components:  $e_{31} = e_{32}$ ,  $e_{33}$ , and  $e_{15} = e_{24}$ . In our superlattice only two of them have large values:  $e_{33}$  and  $e_{15}$ . When approaching the  $P4mm-Cm$  boundary from the tetragonal phase, the  $e_{33}$  value increases monotonically whereas the  $e_{15}$  value diverges critically and reaches the value of  $80 \text{ C/m}^2$  (not shown).

In the orthorhombic phase (in the coordinate system of the reference tetragonal structure) the  $e_{11} = e_{22}$ ,  $e_{12} = e_{21}$ ,  $e_{13} = e_{23}$ ,  $e_{34} = e_{35}$ , and  $e_{16} = e_{26}$  moduli are nonzero, and the total number of

Table 3. Largest piezoelectric moduli for monoclinic phase of free-standing  $(\text{BTO})_1/(\text{STO})_1$  superlattice, for tetragonal phase of the same superlattice grown on  $\text{SrTiO}_3$  substrate, and for tetragonal barium titanate.

Structure	SL1/1		$\text{BaTiO}_3$
	$[xxz]$	$[001]^a$	
$e_{33}, \text{C/m}^2$ ( $d_{33}, \text{pC/N}$ )	31.9 (460)	7.1 (49)	6.3 (42)
$e_{15}, \text{C/m}^2$ ( $d_{15}, \text{pC/N}$ )	-0.09 (-19)	3.2 (31)	-2.9 (-24)

<sup>a</sup>Superlattice grown on  $\text{SrTiO}_3$  substrate.

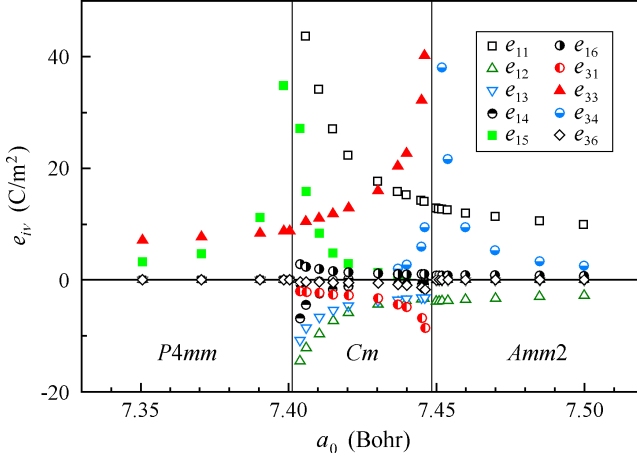


Fig. 5. (Color online) Components of the piezoelectric tensor  $e_{i\nu}$  in polar phases of  $(\text{BTO})_1/(\text{STO})_1$  superlattice as a function of the in-plane lattice parameter  $a_0$ . Vertical lines indicate the phase boundaries.

independent parameters is 5. Among them the  $e_{11}$ ,  $e_{12}$ ,  $e_{34}$ , and  $e_{16}$  moduli have the largest values (see Fig. 5). The only modulus that behaves critically at the boundary between  $Cm$  and  $Amm2$  phases is the  $e_{34}$  one, with a maximum value reaching  $192 \text{ C/m}^2$  (not shown).

The most complex behavior of piezoelectric moduli is observed in the monoclinic phase because the change of the in-plane lattice parameter  $a_0$  results in monotonic rotation of the polarization vector in the  $(\bar{1}10)$  plane. In the coordinate system of the reference tetragonal structure, all 18 components of the  $e_{i\nu}$  tensor are nonzero (the total number of independent parameters is 10). As follows from Fig. 5, in the monoclinic phase the  $e_{11} = e_{22}$ ,  $e_{15} = e_{24}$ ,  $e_{12} = e_{21}$ ,  $e_{13} = e_{23}$ ,  $e_{14} = e_{25}$ , and  $e_{16} = e_{26}$  moduli diverge critically at the boundary between  $Cm$  and  $P4mm$  phases, and  $e_{33}$ ,  $e_{34} = e_{35}$ ,  $e_{31} = e_{32}$ , and  $e_{36}$  moduli diverge critically at the boundary between  $Cm$  and  $Amm2$  phases. It should be noted that when crossing the boundaries, small additional jumps (about  $\sim 10\%$ ) are observed in the  $e_{33}$  modulus (at the  $Cm$ – $P4mm$  boundary) and in  $e_{11}$  and  $e_{12}$  moduli (at the  $Cm$ – $Amm2$  boundary).

### 3.5. Elastic properties

It is known that ferroelectric phase transitions between two polar phases are often the *improper ferroelastic* ones, which means that they are accompanied by appearance of soft *acoustic* modes and spontaneous strain, but the strain is not the

primary order parameter. This occurs when the strain tensor and the polar vector transform according to the same irreducible representation of the high-symmetry phase.<sup>59</sup> As such phase transitions occur in BTO/STO superlattices when changing the in-plane lattice parameter  $a_0$ , it was interesting to study the influence of these phase transitions on the elastic properties of superlattices, especially taking into account that these properties of superlattices have not been studied so far.

In the tetragonal  $P4mm$  phase, the elastic compliance tensor  $S_{\mu\nu}$  ( $\mu, \nu = 1-6$ ) has six independent and nine nonzero components. In the orthorhombic  $Amm2$  phase (in the coordinate system of the reference tetragonal structure) the tensor has nine independent and 13 nonzero components, and in the monoclinic  $Cm$  phase it has 13 independent and 21 nonzero components.

The components of the elastic compliance tensor  $S_{\mu\nu}$  for polar phases of  $(\text{BTO})_1/(\text{STO})_1$  superlattice are plotted as a function of the in-plane lattice parameter  $a_0$  in Fig. 6. It is seen that at the boundary between  $P4mm$  and  $Cm$  phases the components of  $S_{\mu\nu}$  tensor exhibit a step-like change ( $S_{13} = S_{23}$ ,  $S_{33}$ ,  $S_{66}$ ,  $S_{16} = S_{26}$ ,  $S_{36}$ ,  $S_{34} = S_{35}$ ,  $S_{46} = S_{56}$  moduli), a critical divergence from the monoclinic side ( $S_{11} = S_{22}$ ,  $S_{12}$ ,  $S_{15} = S_{24}$ ,  $S_{14} = S_{25}$ ,  $S_{45}$  moduli), or critical divergences from both sides of the boundary ( $S_{44} = S_{55}$  modulus). In the monoclinic phase, the  $S_{14}$ ,  $S_{15}$ ,  $S_{16}$ ,  $S_{34}$ ,  $S_{36}$ ,  $S_{45}$ , and  $S_{46}$  moduli become nonzero. In the orthorhombic phase, the  $S_{14}$ ,  $S_{15}$ ,  $S_{34}$ , and  $S_{46}$  moduli vanish again

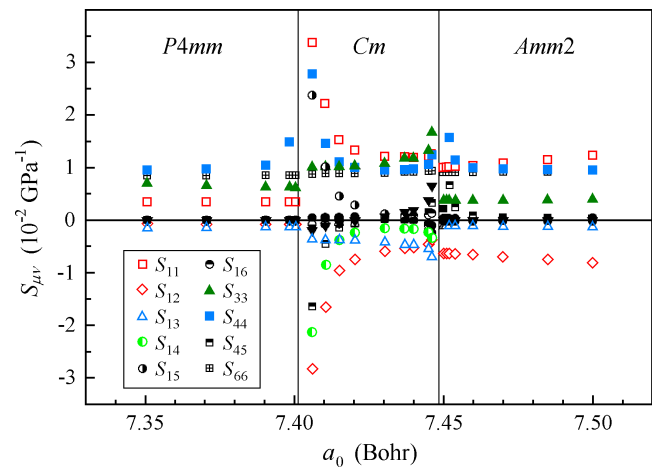


Fig. 6. (Color online) Components of the elastic compliance tensor  $S_{\mu\nu}$  for polar phases of  $(\text{BTO})_1/(\text{STO})_1$  superlattice as a function of the in-plane lattice parameter  $a_0$ . Vertical lines indicate the phase boundaries.

whereas the other moduli remain nonzero. At the boundary between  $Cm$  and  $Amm2$  phases the anomalies in elastic moduli are smaller: the  $S_{11}$ ,  $S_{12}$ , and  $S_{66}$  moduli exhibit step-like changes, the  $S_{13}$ ,  $S_{14}$ ,  $S_{15}$ ,  $S_{16}$ ,  $S_{33}$ ,  $S_{34}$ ,  $S_{36}$ , and  $S_{46}$  moduli exhibit weak divergence from the monoclinic side, and the  $S_{44}$  and  $S_{45}$  moduli exhibit weak divergence from both sides of the boundary.

The critical divergence of the  $S_{44}$  modulus at both  $P4mm-Cm$  and  $Cm-Amm2$  boundaries indicates that the phase transitions induced in the superlattice by the increase of the in-plane lattice parameter are indeed the ferroelastic ones.

### 3.6. Thermodynamic stability

Thermodynamic stability of ferroelectric superlattices is very important for their possible applications. Thermodynamic stability of BTO/STO superlattice is determined by the mixing enthalpy of the superlattice and its relationship with the mixing enthalpy of the disordered  $Ba_{0.5}Sr_{0.5}TiO_3$  solid solution. The most complex part of the first-principles calculation of thermodynamic stability is the calculation of the mixing enthalpy for a solid solution because its simulation using supercells with a large number of randomly distributed atoms makes it extremely time-consuming.

A conceptually new approach to this problem was proposed by Zunger *et al.*<sup>60</sup> In this approach, a disordered solid solution  $A_xB_{1-x}$  is modeled using a special quasirandom structure (SQS) — a short-period superstructure, whose statistical properties (numbers of  $N_{AA}$ ,  $N_{BB}$ , and  $N_{AB}$  atomic pairs in few nearest shells) are as close as possible to those of ideal disordered solid solution (at the same time the sites of the superstructure are deterministically filled with  $A$  and  $B$  atoms). This method has been widely used to study the electronic structure and physical properties of semiconductor solid solutions and the ordering phenomena in metal alloys. To study

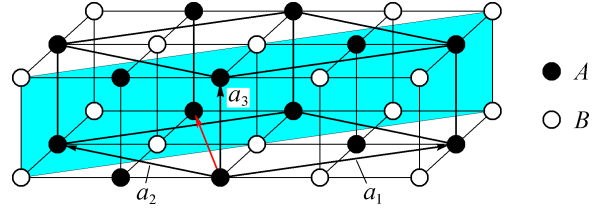


Fig. 7. (Color online) The unit cell of SQS-4b superstructure contains four primitive cells of the perovskite structure and is constructed using  $a_1$ ,  $a_2$ , and  $a_3$  translation vectors. The atoms of one of two types,  $A$  or  $B$ , occupy the sites of one sublattice of the perovskite structure lying on the planes (shown by blue), which are perpendicular to the superlattice axis (shown by red arrow). The stacking sequence of the planes along the superlattice axis is  $AABB$ .

the properties of ferroelectric solid solutions this approach was used quite rare.<sup>61,62</sup>

The structure of the disordered  $Ba_{0.5}Sr_{0.5}TiO_3$  solid solution was modeled using two special quasirandom structures SQS-4 constructed with the **gensqs** program from ATAT toolkit.<sup>63</sup> One of these structures is sketched in Fig. 7. The translation vectors, superlattice axis, and stacking sequence of the planes filled with the same atoms, Ba or Sr (denoted by  $A$  and  $B$ ), are given in Table 4. The pair correlation functions  $\Pi_{2,m}$  ( $m$  is the shell number), which describe the deviation of statistical properties of these SQSs from those of an ideal solid solution, are also given in this table. For  $x = 0.5$   $\Pi_{2,m}$  is simply  $(2N_{AA}/N_m - 1)$ , where  $N_m$  is a number of neighbors in the  $m$ th shell. As follows from this table, for the SQS-4a structure strong deviation from an ideal solid solution appears only in the fourth shell; for the SQS-4b structure deviations appear in the second and fourth shells, but are smaller. The mixing enthalpy  $\Delta H$  for all studied structures  $X$  (superlattices with different periods and SQS structures) was calculated using the formula

$$\Delta H = E_{\text{tot}}(X) - [E_{\text{tot}}(\text{BaTiO}_3) + E_{\text{tot}}(\text{SrTiO}_3)]/2$$

from the values of the total energy  $E_{\text{tot}}$  (per five-atom formula unit) for free-standing fully relaxed

Table 4. Translation vectors, superlattice axis, stacking sequence of atomic planes, and correlation functions  $\Pi_{2,m}$  for SQS-4 structures used for modeling of disordered  $Ba_{0.5}Sr_{0.5}TiO_3$  solid solution.

Structure	Translation vectors	Axis and stacking sequence	$\Pi_{2,1}$	$\Pi_{2,2}$	$\Pi_{2,3}$	$\Pi_{2,4}$
SQS-4a	[211], [112], [121]	$[\bar{1}\bar{1}1]$ $AABB$	0	0	0	-1
SQS-4b	[210], [210], [001]	$[\bar{1}20]$ $AABB$	0	-1/3	0	1/3

Table 5. The mixing enthalpy (in meV) for five  $(\text{BTO})_n/(\text{STO})_n$  superlattices with different periods and two SQS-4 structures used for modeling of disordered  $\text{Ba}_{0.5}\text{Sr}_{0.5}\text{TiO}_3$  solid solution.

SL1/1	SL2/2	SL3/3	SL4/4	SL5/5	SQS-4a	SQS-4b
2.9	8.9	11.4	12.6	13.4	16.8	11.0

paraelectric  $Pm3m$  and  $P4/mmm$  phases. The obtained values of  $\Delta H$  for these structures are given in Table 5.

An unexpected result of our calculation is the fact that  $\Delta H$  values for two shortest-period superlattices (1/1 and 2/2) appeared smaller than  $\Delta H$  values for both realizations of disordered solid solution. This means that a tendency to *short-range ordering* of components exists in the  $\text{BaTiO}_3\text{--SrTiO}_3$  system. Low values of  $\Delta H$  for these superlattices ( $< 9$  meV) indicate that short-period BTO/STO superlattices are thermodynamically stable at 300 K.

The tendency to short-range ordering found in (001)-oriented BTO/STO superlattices can be explained by a general tendency of the  $A$  cations to order in a layered manner in perovskites, in contrast to the  $B$  cations, which prefer a rock-salt ordering.<sup>64</sup> One can add that a similar effect was observed in our studies of (001)-oriented  $(\text{PbTiO}_3)_n/(\text{SrTiO}_3)_n$  superlattices, where *negative* values of  $\Delta H$  for  $n = 1\text{--}3$  and positive values for larger  $n$  were observed.

Our values of the mixing enthalpy for BTO/STO superlattices are much smaller than  $\Delta H$  value obtained in Ref. 65 (42 meV per formula unit). Analysis of the calculation technique used in Ref. 65 shows that atomic positions in the superstructures were not relaxed and the superstructures were assumed to be cubic when calculating the energies of different atomic configurations. So, the calculated mixing enthalpy in this paper includes a large energy of excess strain.

#### 4. Discussion

Our results on the influence of epitaxial strain on the ground state of BTO/STO superlattice agree only partially with the results obtained in Refs. 24, 34, 36, and 37. The results coincide in that: (1) the ground state for free-standing  $(\text{BTO})_1/(\text{STO})_1$  superlattice is the monoclinic  $Cm$  phase, (2) under the compressive strain, the superlattice undergoes the phase transition from  $Cm$  to  $P4mm$  phase, and (3)

the dielectric constant diverges at the  $P4mm\text{--}Cm$  phase boundary. At the same time, in contrast to the results of Refs. 36 and 37, we succeeded to observe the phase transition to the  $Amm2$  orthorhombic phase under the tensile strain (in Refs. 36 and 37 only the rotation of the polarization vector towards the [110] direction was observed under the tensile strain). We consider our results to be more reliable because they agree with the results obtained for strained  $\text{BaTiO}_3$ <sup>2</sup> and  $\text{SrTiO}_3$ <sup>45</sup> thin films, the results of recent atomistic calculations of the strain–temperature phase diagram for  $(\text{BTO})_2/(\text{STO})_2$  superlattice,<sup>38</sup> and with results obtained for another superlattice,  $\text{PbTiO}_3/\text{PbZrO}_3$ .<sup>46</sup> In all these systems the same phase sequence,  $P4mm\text{--}Cm\text{--}Amm2$ , was observed as the in-plane lattice parameter was increased.

The increase in the polarization  $P_s$  in  $(\text{BTO})_n/(\text{STO})_n$  superlattices grown on  $\text{SrTiO}_3$  substrates with increasing the layer thickness  $n$  (Table 2) agrees with the results of Ref. 42 in which the explanation of this phenomenon was proposed. In free-standing superlattices, the  $P_z$  component of polarization also increased with increasing  $n$ , but the  $P_x$  and  $P_y$  components decreased with increasing  $n$ , in contrast to the results observed for 3/3, 4/4, and 5/5 superlattices with fixed in-plane lattice parameter equal to 1.01 times the lattice parameter of  $\text{SrTiO}_3$ .<sup>34</sup> We attribute these changes to the decrease of the in-plane lattice parameter  $a_0$  for free-standing superlattices with increasing  $n$  (see Table 2).

Unfortunately, only a few data points presented in Ref. 37 for the dielectric constant at the  $P4mm\text{--}Cm$  boundary for  $(\text{BTO})_1/(\text{STO})_1$  superlattice did not enabled us to make detailed comparison between our results. However, the comparison of our dielectric data with those calculated for  $(\text{PbTiO}_3)_1/(\text{PbZrO}_3)_1$  superlattice<sup>46</sup> shows that in the monoclinic phase all eigenvalues of the  $\varepsilon_{ij}$  tensor for BTO/STO superlattice are higher, and so this superlattice may be more promising for different applications.

To obtain large piezoelectric moduli necessary for technological applications, the epitaxial strain in the BTO/STO superlattice should be tuned to a value at which  $e_{i\nu}$  and  $S_{\mu\nu}$  properties of the superlattice diverge. As was shown in Secs. 3.4 and 3.5, this appears at the phase boundaries. The calculations show that in the vicinity of the  $P4mm\text{--}Cm$  boundary the  $d_{11}$  piezoelectric coefficient reaches a maximum value of 2300 pC/N in the monoclinic phase and the  $d_{15}$  coefficient reaches a value of 6200 pC/N in the tetragonal phase. In the vicinity of

the  $Cm$ – $Amm2$  boundary, the  $d_{33}$  piezoelectric coefficient reaches a value of 920 pC/N in the monoclinic phase and the  $d_{34}$  coefficient reaches a value of 10500 pC/N in the orthorhombic phase. For comparison, the maximum piezoelectric coefficient obtained experimentally on single crystals of the Pb  $(Zn_{1/3}Nb_{2/3})O_3$ –PbTiO<sub>3</sub> system was 2500 pC/N.<sup>66</sup> Anomalous increase in the calculated  $d_{15}$  and  $d_{33}$  coefficients up to  $\sim 8500$  pC/N was predicted for hydrostatically stressed PbTiO<sub>3</sub> in the vicinity of the  $P4mm$ – $Cm$  phase boundary.<sup>67</sup>

Consider now the elastic properties of BTO/STO superlattice and the results indicating the appearance of improper ferroelastic phase transitions. According to Ref. 59, in crystals with  $P4mm$  space group the phase transition  $P4mm \rightarrow m$  should be of the ferroelastic type. The spontaneous strain at this phase transition is characterized by one or both nonzero  $u_4$  and  $u_5$  components of the strain tensor, and a soft transverse acoustic (TA) mode with a wave vector parallel to the polar axis should appear in the phonon spectrum in the vicinity of the  $\Gamma$  point. Direct calculations of frequencies of acoustic modes in the tetragonal phase at the point with a reduced wave vector  $\mathbf{q} = (0, 0, 0.05)$  confirmed this (see Fig. 8): when approaching the  $P4mm$ – $Cm$  boundary, the frequency of a doubly degenerate TA phonon with the  $\Lambda_5$  symmetry decreased by five times. The softening of this mode is directly related to the divergence of the  $S_{44} = S_{55}$  components of the elastic compliance tensor.

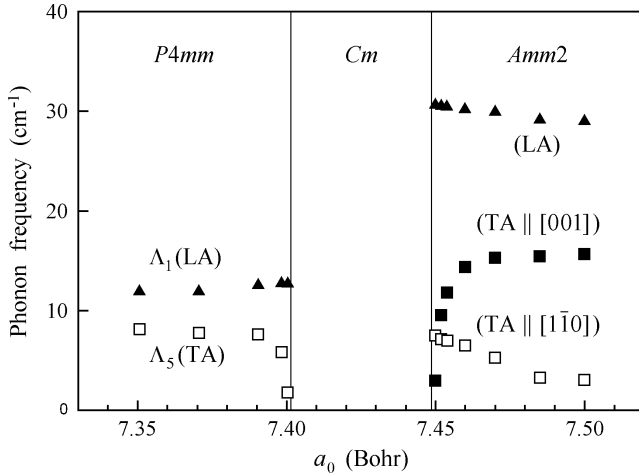


Fig. 8. Frequencies of acoustic modes in the vicinity of the  $\Gamma$  point in polar phases of  $(BTO)_1/(STO)_1$  superlattice as a function of the in-plane lattice parameter  $a_0$ . Vertical lines indicate the phase boundaries.

At the boundary between  $Cm$  and  $Amm2$  phases, there should be another ferroelastic phase transition. According to Ref. 59, the transition  $mm2 \rightarrow m$  is accompanied by spontaneous strain with one nonzero of three  $u_4, u_5, u_6$  components. In our coordinate system with unusual for orthorhombic phase orientation of the polar axis (along the  $[110]$  direction) there should be a softening of TA phonon with a wave vector oriented along this axis. This was confirmed by direct calculations of frequencies of acoustic modes at the point in the Brillouin zone with a reduced wave vector  $\mathbf{q} = (0.035, 0.035, 0)$  (see Fig. 8). In contrast to the tetragonal phase in which the soft acoustic mode is doubly degenerate, in the orthorhombic phase the only phonon mode that softens at the phase boundary is the TA mode polarized along the  $[001]$  axis. In our opinion, this difference is the reason why the anomalies in the elastic properties at the ferroelastic  $Cm$ – $Amm2$  phase transition are much weaker than those at the ferroelastic  $P4mm$ – $Cm$  phase transition. Unusual orientation of the polar axis in our coordinate system results in coupling of some components of the elastic compliance tensor: for example, the  $S_{44}$  and  $S_{45}$  moduli, which diverge in the orthorhombic phase, satisfy the relation  $S_{44} - S_{45} \approx \text{const.}$  in this phase.

Negative value of the acoustic phonon frequency in the  $Cm$  phase, which is seen in a narrow wave vector region in Fig. 1, is an artifact of calculations. Computation of the phonon dispersion curves in the vicinity of the  $\Gamma$  point revealed three acoustic branches  $\omega(q)$ , whose frequencies increased monotonically with increasing  $q$ , but gave negative values of  $\omega(0)$  (about  $8 \text{ cm}^{-1}$ ) in the limit  $q \rightarrow 0$  because of numerical errors. After application of the acoustic sum rule,  $\omega(0)$  restored its zero value, but the derivative  $d\omega/dq$  near  $q = 0$  for the softest mode became negative. So, there is no contradiction between the phonon spectra and the positive definiteness of the elastic moduli matrix  $C_{ij}$  calculated in Sec. 3.5.

## 5. Conclusion

In this work, the properties of  $(001)$ -oriented  $(BaTiO_3)_m/(SrTiO_3)_n$  superlattices with  $m = n = 1-4$  were calculated using the first-principles density functional theory. For free-standing superlattices, the ground state is the monoclinic  $Cm$  polar phase. Under the in-plane compressive epitaxial strain, it transforms to tetragonal polar  $P4mm$  phase,

and under in-plane tensile strain, it transforms to orthorhombic  $Amm2$  polar phase. All components of the static dielectric tensor ( $\epsilon_{ij}$ ), the piezoelectric tensor ( $e_{iv}$ ), and the elastic compliance tensor ( $S_{\mu\nu}$ ) were calculated as a function of the in-plane lattice parameter for 1/1 superlattice. The critical behavior of some components of  $\epsilon_{ij}$ ,  $e_{iv}$ , and  $S_{\mu\nu}$  tensors at the boundaries between different polar phases was observed. It was shown that the phase transitions between different polar phases are of the improper ferroelastic type. The possibility of obtaining ultra-high piezoelectric moduli using fine tuning of the epitaxial strain in superlattices was demonstrated. The comparison of the mixing enthalpy calculated for superlattices and disordered  $Ba_{0.5}Sr_{0.5}TiO_3$  solid solution modeled using two special quasirandom structures SQS-4 revealed a tendency of the  $BaTiO_3$ – $SrTiO_3$  system to short-range ordering of cations and showed that short-period superlattices are thermodynamically quite stable.

## Acknowledgment

This work was supported by the RFBR Grant No. 08-02-01436.

## References

1. N. A. Pertsev, A. G. Zembilgotov and A. K. Tagantsev, *Phys. Rev. Lett.* **80**, 1988 (1998).
2. O. Diéguez, S. Tinte, A. Antons, C. Bungaro, J. B. Neaton, K. M. Rabe and D. Vanderbilt, *Phys. Rev. B* **69**, 212101 (2004).
3. J. H. Haeni, P. Irvin, W. Chang, R. Uecker, P. Reiche, Y. L. Li, S. Choudhury, W. Tian, M. E. Hawley, B. Craigo *et al.*, *Nature* **430**, 758 (2004).
4. M. Dawber, K. M. Rabe and J. F. Scott, *Rev. Mod. Phys.* **77**, 1083 (2005).
5. K. Iijima, T. Terashima, Y. Bando, K. Kamigaki and H. Terauchi, *J. Appl. Phys.* **72**, 2840 (1992).
6. E. Wiener-Avnear, *Appl. Phys. Lett.* **65**, 1784 (1994).
7. H. Tabata, H. Tanaka and T. Kawai, *Appl. Phys. Lett.* **65**, 1970 (1994).
8. H. Tabata and T. Kawai, *Appl. Phys. Lett.* **70**, 321 (1997).
9. B. D. Qu, M. Evstigneev, D. J. Johnson and R. H. Prince, *Appl. Phys. Lett.* **72**, 1394 (1998).
10. T. Zhao, Z.-H. Chen, F. Chen, W.-S. Shi, H.-B. Lu and G.-Z. Yang, *Phys. Rev. B* **60**, 1697 (1999).
11. O. Nakagawara, T. Shimuta, T. Makino, S. Arai, H. Tabata and T. Kawai, *Appl. Phys. Lett.* **77**, 3257 (2000).
12. T. Tsurumi, T. Ichikawa, T. Harigai, H. Kakemoto and S. Wada, *J. Appl. Phys.* **91**, 2284 (2002).
13. T. Shimuta, O. Nakagawara, T. Makino, S. Arai, H. Tabata and T. Kawai, *J. Appl. Phys.* **91**, 2290 (2002).
14. J. Kim, Y. Kim, Y. S. Kim, J. Lee, L. Kim and D. Jung, *Appl. Phys. Lett.* **80**, 3581 (2002).
15. L. Kim, D. Jung, J. Kim, Y. S. Kim and J. Lee, *Appl. Phys. Lett.* **82**, 2118 (2003).
16. S. Rios, A. Ruediger, A. Q. Jiang, J. F. Scott, H. Lu and Z. Chen, *J. Phys.: Condens. Matter* **15**, L305 (2003).
17. A. Q. Jiang, J. F. Scott, H. Lu and Z. Chen, *J. Appl. Phys.* **93**, 1180 (2003).
18. F. Q. Tong, W. X. Yu, F. Liu, Y. Zuo and X. Ge, *Mater. Sci. Eng. B* **98**, 6 (2003).
19. T. Harigai, D. Tanaka, H. Kakemoto, S. Wada and T. Tsurumi, *J. Appl. Phys.* **94**, 7923 (2003).
20. T. Tsurumi, T. Harigai, D. Tanaka, H. Kakemoto and S. Wada, *Sci. Technol. Adv. Mater.* **5**, 425 (2004).
21. R. R. Das, Y. I. Yuzyuk, P. Bhattacharya, V. Gupta and R. S. Katiyar, *Phys. Rev. B* **69**, 132302 (2004).
22. R. S. Katiyar, Y. I. Yuzyuk, R. R. Das, P. Bhattacharya and V. Gupta, *Ferroelectrics* **329**, 3 (2005).
23. D. A. Tenne, A. Bruchhausen, N. D. Lanzillotti-Kimura, A. Fainstein, R. S. Katiyar, A. Cantarero, A. Soukiasian, V. Vaithyanathan, J. H. Haeni, W. Tian *et al.*, *Science* **313**, 1614 (2006).
24. J. Lee, L. Kim, J. Kim, D. Jung and U. V. Waghmare, *J. Appl. Phys.* **100**, 051613 (2006).
25. W. Tian, J. C. Jiang, X. Q. Pan, J. H. Haeni, Y. L. Li, L. Q. Chen, D. G. Schlom, J. B. Neaton, K. M. Rabe and Q. X. Jia, *Appl. Phys. Lett.* **89**, 092905 (2006).
26. T. Harigai, H. Kimbara, H. Kakemoto, S. Wada and T. Tsurumi, *Ferroelectrics* **357**, 128 (2007).
27. B. R. Kim, T.-U. Kim, W.-J. Lee, J. H. Moon, B.-T. Lee, H. S. Kim and J. H. Kim, *Thin Solid Films* **515**, 6438 (2007).
28. B. Strukov, S. Davitadze, V. Lemanov, S. Shulman, Y. Uesu, S. Asanuma, D. Schlom and A. Soukiasian, *Ferroelectrics* **370**, 57 (2008).
29. A. Bruchhausen, A. Fainstein, A. Soukiasian, D. G. Schlom, X. X. Xi, M. Bernhagen, P. Reiche and R. Uecker, *Phys. Rev. Lett.* **101**, 197402 (2008).
30. J. Hlinka, V. Železný, S. M. Nakhmanson, A. Soukiasian, X. X. Xi and D. G. Schlom, *Phys. Rev. B* **82**, 224102 (2010).
31. N. Ortega, A. Kumar, O. A. Maslova, Y. I. Yuzyuk, J. F. Scott and R. S. Katiyar, *Phys. Rev. B* **83**, 144108 (2011).
32. O. A. Maslova, Y. I. Yuzyuk, N. Ortega, A. Kumar and R. S. Katiyar, *Phys. Solid State* **53**, 1062 (2011).

33. J. B. Neaton and K. M. Rabe, *Appl. Phys. Lett.* **82**, 1586 (2003).
34. K. Johnston, X. Huang, J. B. Neaton and K. M. Rabe, *Phys. Rev. B* **71**, 100103 (2005).
35. L. Kim, J. Kim, U. V. Waghmare, D. Jung and J. Lee, *Integ. Ferroelectr.* **73**, 3 (2005).
36. L. Kim, J. Kim, D. Jung, J. Lee and U. V. Waghmare, *Appl. Phys. Lett.* **87**, 052903 (2005).
37. L. Kim, J. Kim, U. V. Waghmare, D. Jung and J. Lee, *Phys. Rev. B* **72**, 214121 (2005).
38. S. Lisenkov and L. Bellaiche, *Phys. Rev. B* **76**, 020102 (2007).
39. J. H. Lee, U. V. Waghmare and J. Yu, *J. Appl. Phys.* **103**, 124106 (2008).
40. Z. Y. Zhu, H. Y. Zhang, M. Tan, X. H. Zhang and J. C. Han, *J. Phys. D: Appl. Phys.* **41**, 215408 (2008).
41. S. Lisenkov, I. Ponomareva and L. Bellaiche, *Phys. Rev. B* **79**, 024101 (2009).
42. J. H. Lee, J. Yu and U. V. Waghmare, *J. Appl. Phys.* **105**, 016104 (2009).
43. A. I. Lebedev, *Phys. Solid State* **51**, 2324 (2009).
44. A. I. Lebedev, *Phys. Solid State* **52**, 1448 (2010).
45. A. Antons, J. B. Neaton, K. M. Rabe and D. Vanderbilt, *Phys. Rev. B* **71**, 024102 (2005).
46. C. Bungaro and K. M. Rabe, *Phys. Rev. B* **69**, 184101 (2004).
47. G. Sághi-Szabó, R. E. Cohen and H. Krakauer, *Phys. Rev. B* **59**, 12771 (1999).
48. A. I. Lebedev, *Phys. Solid State* **51**, 362 (2009).
49. X. Gonze, J.-M. Beuken, R. Caracas, F. Detraux, M. Fuchs, G.-M. Rignanese, L. Sindic, M. Verstraete, G. Zerah, F. Jollet *et al.*, *Comput. Mater. Sci.* **25**, 478 (2002).
50. J. P. Perdew and A. Zunger, *Phys. Rev. B* **23**, 5048 (1981).
51. A. M. Rappe, K. M. Rabe, E. Kaxiras and J. D. Joannopoulos, *Phys. Rev. B* **41**, 1227 (1990).
52. Opium—pseudopotential generation project, <http://opium.sourceforge.net/>.
53. N. J. Ramer and A. M. Rappe, *Phys. Rev. B* **59**, 12471 (1999).
54. G.-M. Rignanese, X. Gonze and A. Pasquarello, *Phys. Rev. B* **63**, 104305 (2001).
55. R. D. King-Smith and D. Vanderbilt, *Phys. Rev. B* **47**, 1651 (1993).
56. H. Fu and R. E. Cohen, *Nature* **403**, 281 (2000).
57. R. Guo, L. E. Cross, S.-E. Park, B. Noheda, D. E. Cox and G. Shirane, *Phys. Rev. Lett.* **84**, 5423 (2000).
58. Z. Wu and H. Krakauer, *Phys. Rev. B* **68**, 014112 (2003).
59. R. Blinc and B. Žekš, *Soft Modes in Ferroelectrics and Antiferroelectrics* (North-Holland Publishing Company, Amsterdam, 1974).
60. A. Zunger, S.-H. Wei, L. G. Ferreira and J. E. Bernard, *Phys. Rev. Lett.* **65**, 353 (1990).
61. B. P. Burton and E. Cockayne, *Ferroelectrics* **270**, 173 (2002).
62. S. A. Prosandeev, E. Cockayne, B. P. Burton, S. Kamba, J. Petzelt, Yu. Yuzyuk, R. S. Katiyar and S. B. Vakhrushev, *Phys. Rev. B* **70**, 134110 (2004).
63. A. van de Walle and G. Ceder, *J. Phase Equilibria* **23**, 348 (2002).
64. G. King and P. M. Woodward, *J. Mater. Chem.* **20**, 5785 (2010).
65. D. Fuks, S. Dorfman, S. Piskunov and E. A. Kotomin, *Phys. Rev. B* **71**, 014111 (2005).
66. S.-E. Park and T. R. ShROUT, *J. Appl. Phys.* **82**, 1804 (1997).
67. Z. Wu and R. E. Cohen, *Phys. Rev. Lett.* **95**, 037601 (2005).